Supporting Information

Growth Mechanism of Epitaxial $SrTiO_3$ on (1×2)+(2×1) reconstructed Sr(1/2 ML)/Si(001) surface

Matjaž Spreitzer,*[,a,‡] Dejan Klement,[a,‡1] Ricardo Egoavil,[b] Jo Verbeeck,[b] Janez Kovač,[c] Anže Založnik,[d] Gertjan Koster,[e,a] Gustaaf Van Tendeloo,[b] Danilo Suvorov,[a] Guus Rijnders[e]

[a]Advanced Materials Department, Jožef Stefan Institute, Jamova 39, 1000 Ljubljana, Slovenia
[b]Electron Microscopy for Materials Science, University of Antwerp, Groenenborgerlaan 171, B-2020 Antwerp, Belgium
[c]Department of Surface Engineering and Optoelectronics, Jožef Stefan Institute, Jamova 39, 1000 Ljubljana, Slovenia
[d]Department for Low and Medium Energy Physics, Jožef Stefan Institute, Jamova 39, 1000 Ljubljana, Slovenia
[e]Faculty of Science & Technology and MESA+ Institute for Nanotechnology, University of Twente, Carré, 3243, 7500 AE Enschede, The Netherlands

[1] Present address: Krka, d. d., Novo mesto, Slovenia

Optimization of background gas pressure

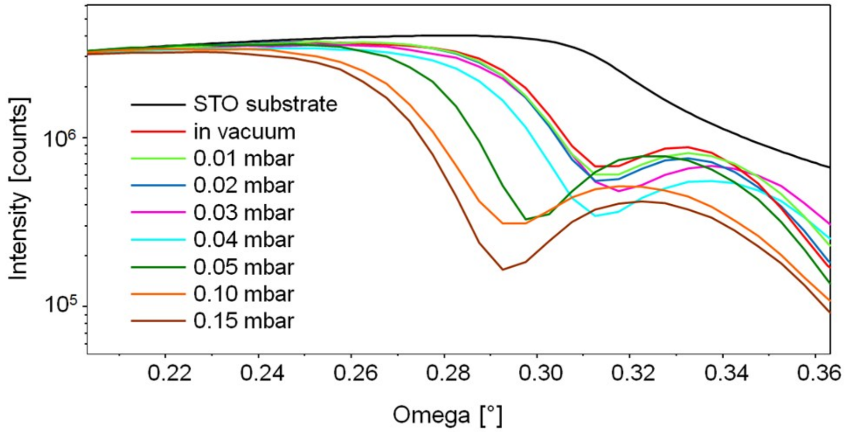

Figure S.1. Comparison of initial part of X-ray reflectivity curves for samples prepared at different Ar background pressures in terms of critical angle ω_c. Density increases from the left (brown curve) to the right (black curve).

Figure S.2 shows Fourier plot for the sample prepared in vacuum. Three peaks can be observed which correspond to separations of three pairs of interfaces. Peak at 39.4 nm is related to the STO layer, while peak at 2.5 nm corresponds to interface layer, which formed due to reaction between Si and STO. Third peak at 41.9 nm is related to the total thickness. Additional layer at the interface was detected also for the sample prepared at 0.01 mbar Ar pressure, while only one peak was observed in the Fourier plot for all the other samples. This does not necessarily mean that there is no interface layer present for the samples deposited at pressures higher than 0.01 mbar. Under circumstances of a limited dynamical range the reflectivity curve can be misinterpreted by a clean interface. In our case, small sample size significantly reduced the dynamical range, which resulted in higher limit for the determination of a thin interface layer. Table S.1 includes also the results of thickness calculations based on direct method. Several different thicknesses were determined for each sample, depending on which two fringes were selected for calculation. Averaging over more fringes generally leads to more accurate results.

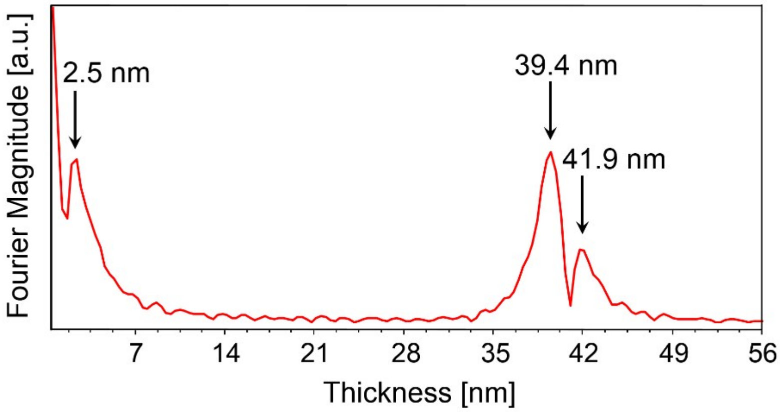

Figure S.2. Fourier magnitude versus thickness plot for the sample prepared in vacuum (app. 1×10^{-8} mbar). Peak positions give thickness information.

Table S.1. Density and layer thickness of STO/Si samples prepared at different argon background gas pressures.

Argon pressure [mbar]		vac.	0.01	0.02	0.03	0.04	0.05	0.10	0.15
Density [g cm^{-3}]		4.34	4.26	4.25	4.25	4.09	3.78	3.51	3.39
Fourier method [nm]	STO layer	39.4	36.6	38.3	37.0	36.2	35.7	33.4	31.5
	Interface layer	2.5	2.3	n.d.	n.d.	n.d.	n.d.	n.d.	n.d.
	Total thickness	41.9	39	38.3	37.0	36.2	35.7	33.4	31.5
Direct method [nm]	1. and 2. fringe	46.6	39.3	38.9	38.4	37.2	36	33.4	32.6
	1. and 3. fringe	43.8	38.4	38.7	38.0	36.7	35.8	33.1	31.9
	1. and 4. fringe	42.8	38.2	38.6	37.7	36.6	35.3	33.2	31.3
	1. and 5. fringe	42.2	38.1	38.3	37.6	36.4	35.3	33.3	30.9
	1. and 6. fringe	41.6	37.6	38.1	37.3	36.3	35.5	33.5	/
	1. and 7. fringe	41.2	37.5	38.1	37.2	36.1	35.5	/	/

* n.d. . . . . . . not detected

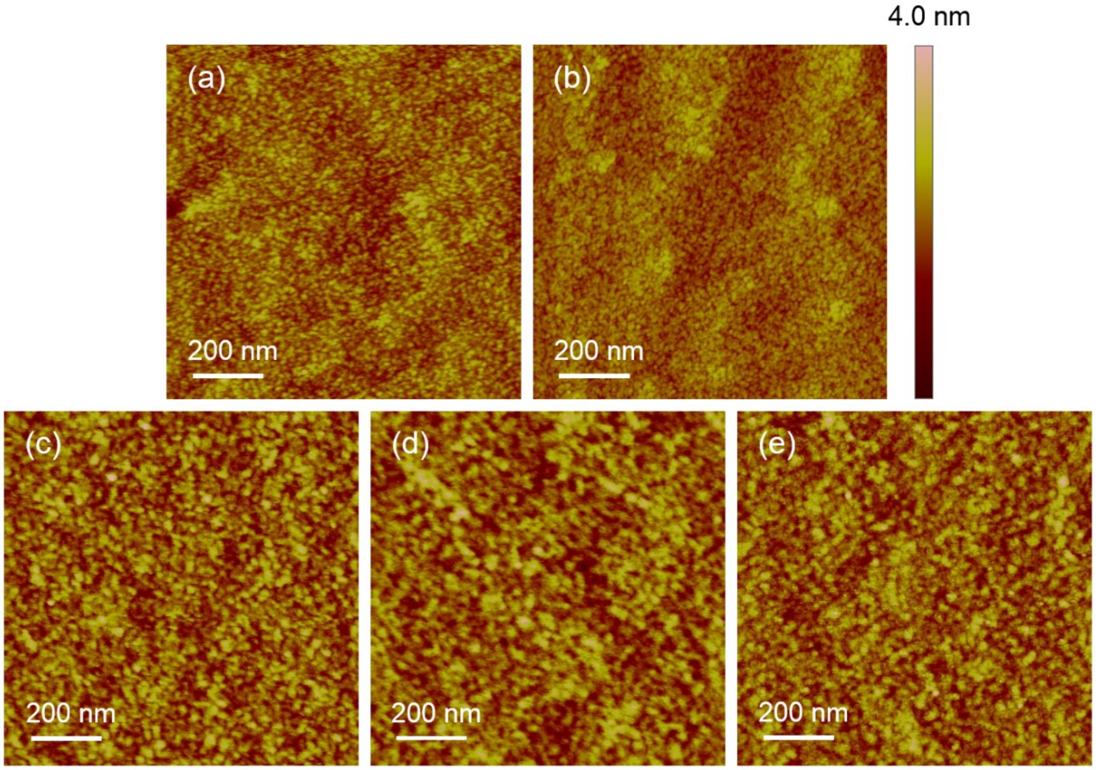

Figure S.3. AFM images of STO thin films deposited at room temperature and (a) in vacuum, (b) at 0.01 mbar, (c) 0.05 mbar, (d) 0.1 mbar, (e) 0.15 mbar Ar pressure. The lateral scan size is 1×1 μm^2.

In order to be able to observe the interface region by means of XPS studies separate samples with STO thickness of 4.5 nm were prepared at the same conditions. The number of pulses required for 4.5 nm thick STO layers was obtained from the thickness analysis of reflectivity curves presented in Figure 1. Figure 2a shows a series of detailed scans for different samples in the Si 2p region with all the spectra aligned for the Si 2p signal from the non-treated substrate (black curve on top). In XPS spectra of the samples prepared in vacuum and at 0.01 mbar two types of chemically bonded Si were found. Beside the elementary Si presented by a doublet Si 2p$_{1/2}$ and Si 2p$_{3/2}$, there exists also a broad peak at higher binding energy (Figure 2b). From the comparison with the spectrum for Si substrate covered with the native oxide layer it is clear that this additional peak is not related to SiO$_2$. Based on the literature it can be explained by silicate phase, which in our case forms due to the interface mixing and reaction of high-energetic species from the plasma plume with the Si substrate. Samples deposited at 0.05, 0.10 and 0.15 mbar Ar pressures exhibit the same XPS spectra where beside the elementary Si no other types of chemically bonded Si were observed, indicating the stable interface between the STO and Si.

Optimization of laser fluence

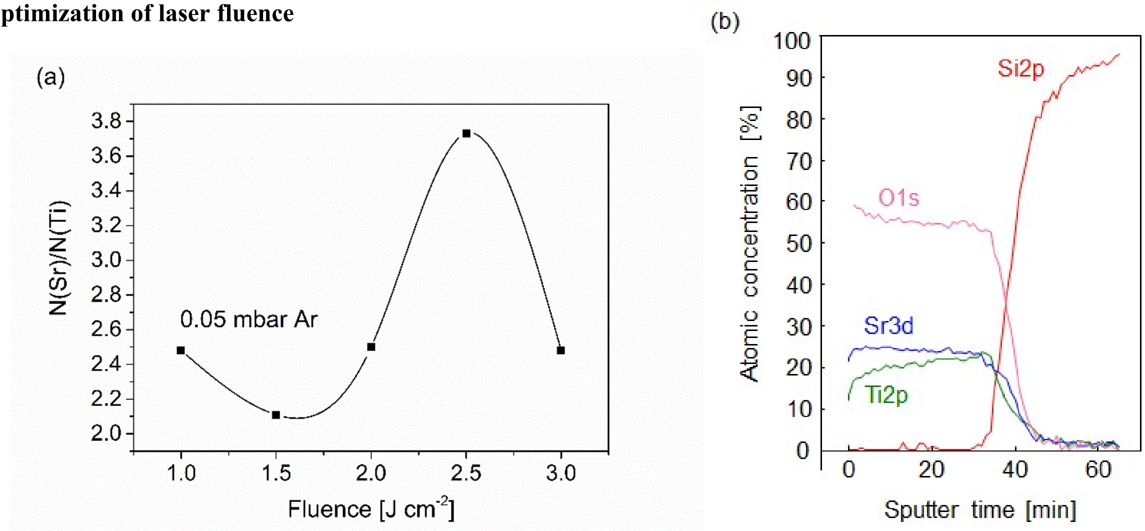

Figure S.4. (a) Sr/Ti atomic ratio in STO films deposited at different fluences determined by XPS. (b) XPS depth profiles obtained on the sample deposited at room temperature, 0.05 mbar Ar pressure and 1.5 J cm^{-2}. Due to carbon contamination results of the topmost layer are not included.

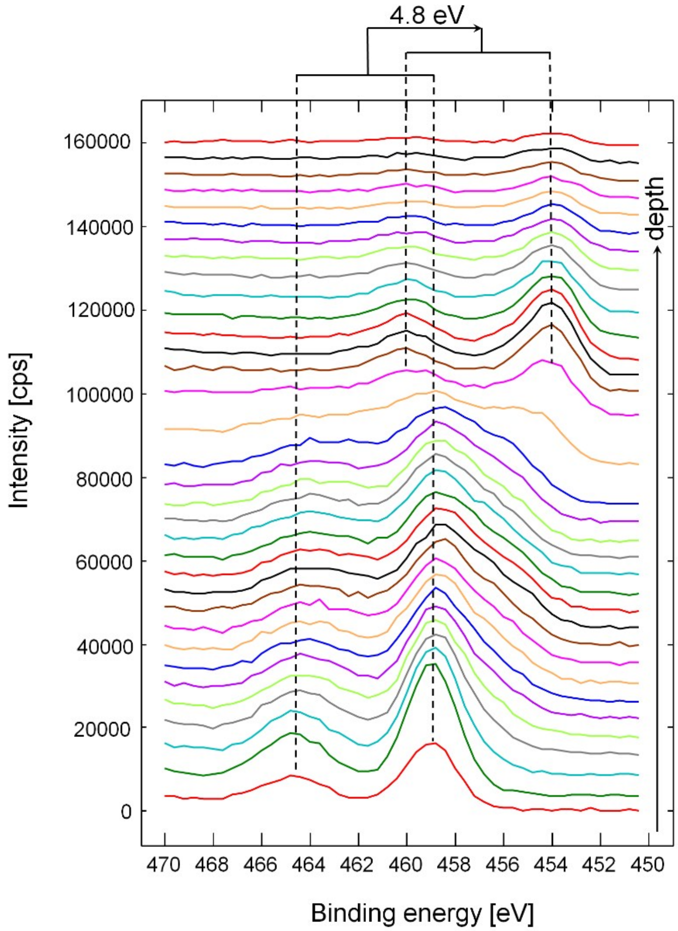

Figure S.5. Ti 2p XPS spectra obtained at different depths during XPS depth profiling of the STO layer deposited at room temperature and 0.05 mbar Ar pressure. Left and right peaks in each of the spectrum correspond to the photoemission from the Ti 2p$_{1/2}$ and Ti 2p$_{3/2}$ energy levels, respectively.

Final deposition of STO

First, clean (free of carbon) reconstructed Si(001) surface was prepared by flashing the substrate to 1200°C for 1.5 min. In the next step 1/2 ML of Sr was deposited on clean Si(001) at 700°C to form the Sr-buffer layer with (1×2)+(2×1) reconstruction. The substrate temperature was then reduced to room temperature where deposition of STO seed layer was initiated. The deposition procedure for the seed layer was derived from detailed studies of initial deposition conditions and is as follows. First, ~1 ML of amorphous STO layer with the right stoichiometry (fluence=1.5 J cm^{-2}) was grown at room temperature and 0.05 mbar Ar pressure, preventing the formation of silicate at the interface. The number of pulses required for 1 ML was determined from XRR measurement. Then, the Ar was removed from the growth chamber and oxygen was introduced to a partial pressure of 1.1×10^{-7} mbar for 5 min in order to oxidize Ti and Sr. Deposition of the second and third ML of STO was performed at the same conditions as the first one. The only difference was in the oxidation step, which was conducted at slightly higher oxygen pressure of 9.3×10^{-7} mbar. After the oxidation of the last (third) ML of STO oxygen was removed from the growth chamber and the 3 MLs thick seed layer was slowly heated up in vacuum (~1×10^{-8} mbar) to the temperature of 517°C for 15 min to crystallize it. We continued with the growth of the STO seed layer. Again, 3 MLs thick STO layer was deposited at room temperature and 0.05 mbar Ar pressure in parts of 1 ML with intermediate 5 min long oxidation periods at 9.3×10^{-7} mbar. The deposition step was followed by crystallization step as already described for the first 3 MLs. These two steps were then repeated until achieving the desired seed layer thickness of 15 MLs. Normally, to grow crystalline oxides, one needs both a high temperature and sufficiently high oxygen pressure. But because simultaneous use of those two conditions lead to oxidation of the silicon, we had to separate them in time. Once the crystalline STO seed layer was formed in this way, additional STO was deposited on top of it in much faster growth regime. This subsequent STO was deposited at temperature of 517°C and 1.3×10^{-6} mbar oxygen pressure. The amount of oxygen pressure was selected according to investigation done by Heyd et al.[1] They showed that the minimum pressure for complete oxidation of Ti at growth speed of about one ML per minute amounts to around $1.3\text{-}2.7\times10^{-6}$ mbar. In total 7366 pulses were deposited during the subsequent STO growth with the repetition rate of 1 Hz. For the sake of clarity schematic drawing of complete fabrication procedure is shown in Figure S.6.

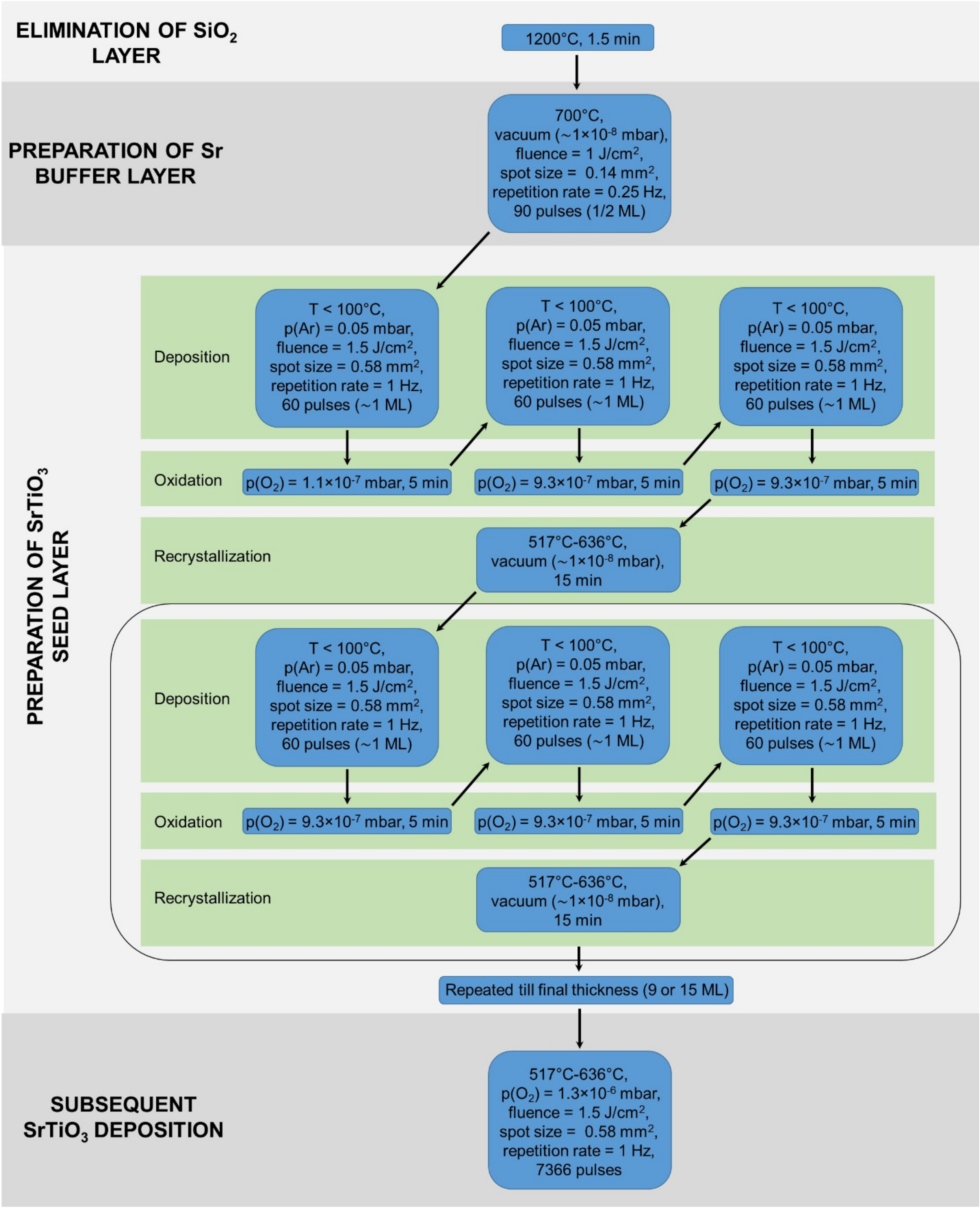

Figure S.6. Complete experimental procedure for the preparation of STO layers on Si(001).

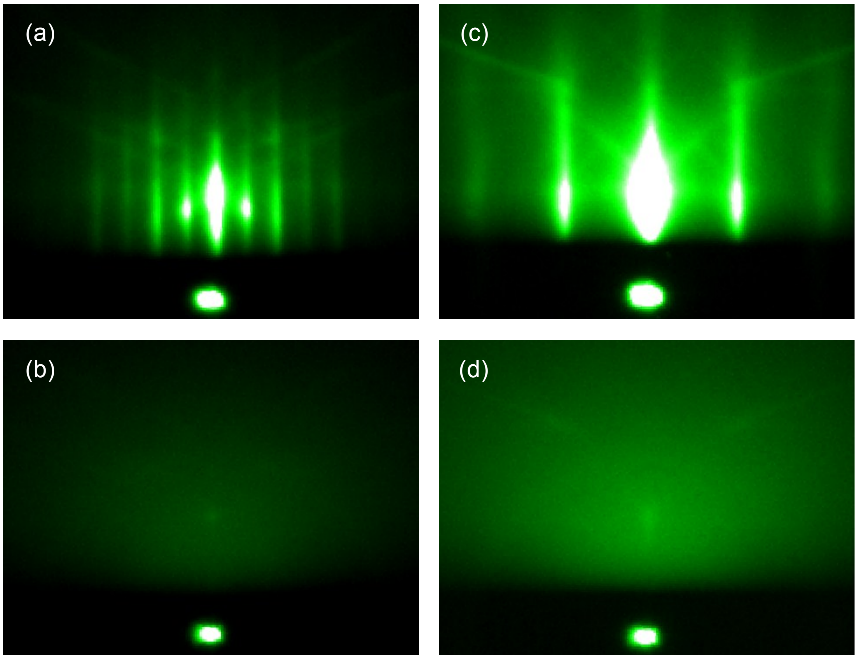

Figure S.7. RHEED patterns in the [110] (a, b) and [100] (c, d) azimuth of Sr-buffered Si taken before the deposition of the STO seed layer (a, c) and after the deposition of 3 ML (b, d) of STO at room temperature.

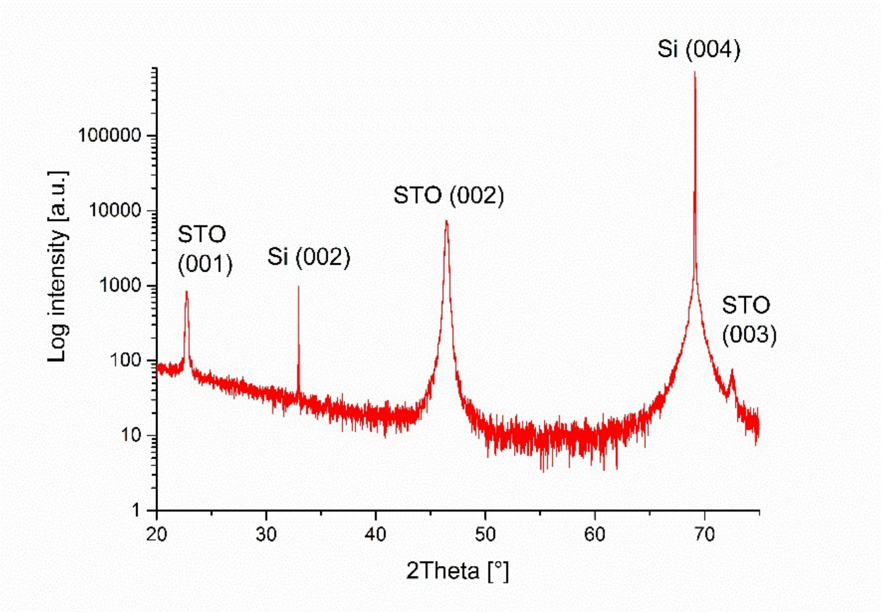

Figure S.8. XRD 2Theta/Theta scan of STO/Si sample after the final deposition.

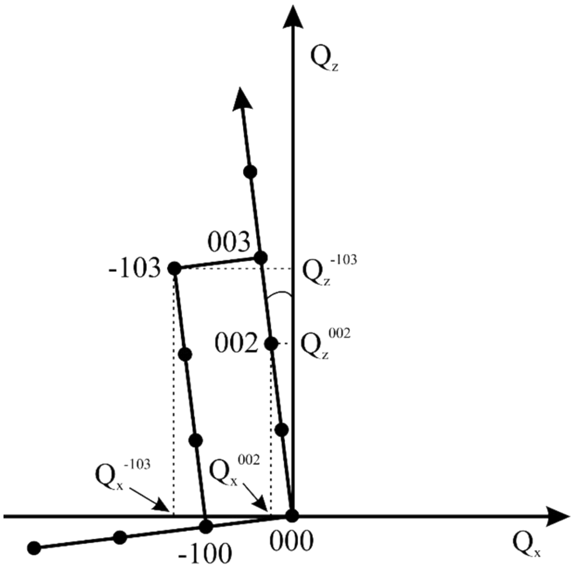

Figure S.9. Illustration of how lattice parameters can be obtained from measurement of two reciprocal lattice spots where there is a layer tilt.

The coordinates of the center (Q_x, Q_z) of both reciprocal lattice spots were determined by Epitaxy software (PANalytical B. V., The Netherlands, Version 4.3a). Then the unit cell parameters were calculated using the equations (1.1) and (1.2).

$$d_{001} = \frac{1}{Q^{001}} = \left[\left(Q_z^{001}\right)^2 + \left(Q_x^{001}\right)^2\right]^{-\frac{1}{2}} = \left[\left(\frac{1}{2}Q_z^{002}\right)^2 + \left(\frac{1}{2}Q_x^{002}\right)^2\right]^{-\frac{1}{2}} \tag{1.1}$$

$$d_{-100} = \frac{1}{Q^{-100}} = \left[\left(\frac{3 \times Q_z^{002}}{2} - Q_z^{-103}\right)^2 + \left(Q_x^{-103} - \frac{3 \times Q_x^{002}}{2}\right)^2\right]^{-\frac{1}{2}} \tag{1.2}$$

The accuracy of the measurement was estimated by taking into account the precision by which the coordinates of the reciprocal lattice spot maxima were determined. This precision is significantly limited by relatively large full width at half maximum (FWHM) of the STO reflections. It is clear that the STO unit cell is larger than that of STO bulk single crystal (3.905 Å). There are two possible reasons for unit cell expansion, nonstoichiometry in STO thin film and strain. The strain can arise from lattice mismatch or thermal expansion mismatch between STO and Si. The lattice mismatch gives rise to compressive strain of 1.66% when STO layer is coherently epitaxial. In this state the layer is in total registry with the substrate across the layer/substrate interface and is called also fully or commensurately strained. In our case, the contribution of the strain induced by the lattice mismatch can be completely excluded because the STO layer thickness (~46 nm) is far above the critical thickness of STO on Si, which was experimentally found to be approximately 2 nm (5 MLs).[2-3] Above the critical thickness STO begins to relax, while the first 5 MLs maintain their registry with the Si substrate. Warusawithana et al. demonstrated that as the film thickness increases, the relative integrated intensity of sharp peak, corresponding to coherently strained STO, decreases while that of a broad peak, corresponding to relaxed STO, increases. Such behaviour clearly shows the transition from mostly commensurate STO to mostly relaxed STO as the film thickness is increased. After approximately 25 MLs (~10 nm) of STO the only observable feature in RSM is broad peak representing completely relaxed STO layer.[3] Therefore, in our case the strain originates exclusively from thermal expansion mismatch.

The thermal expansion coefficient of Si is $\alpha_{Si}=2.6\times10^{-6}$ K^{-1} while the one of STO is $\alpha_{STO}=8.8\times10^{-6}$ K^{-1}.[4] In other words at the growth temperature a semiconductor is slightly larger than what it is at room temperature, while the oxide is significantly larger, and thus one can expect large in-plane tensile strain to develop in the film upon cooling. At the growth temperature of 517°C the bulk unit-cell parameter of STO is given by:

$$a_{bulk\ STO}^{517°C} = a_{bulk\ STO}^{20°C}\left[1 + \alpha_{STO}(517 - 20)\right] = 3.922\ \text{Å} \qquad (1.3)$$

For the bulk unit-cell parameter of STO at room temperature ($a_{bulk\ STO}^{20°C}$) value of 3.905 Å was taken. Equation (1.3) also gives the lattice parameter of the completely relaxed STO layer grown on Si at 517°C. When the temperature is ramped from the growth temperature down to the ambient temperature (23°C) after growth, the lattice parameters of both Si and STO are reduced. The contraction for the Si substrate is driven by α_{Si} while in the case of freestanding STO layer it is driven by α_{STO}. However, in the case of STO thin film on Si the thickness of the STO layer is negligible as compared to the one of the substrate, which results in the contraction of the in-plane lattice parameter of the oxide layer driven by the thermal coefficient of Si. The in-plane STO lattice parameter at ambient temperature can therefore be calculated by Eq. (1.4).

$$a_{STO}^{23°C} = a_{STO}^{517°C}\left[1 + \alpha_{Si}(23 - 517)\right] = 3.917\ \text{Å} \qquad (1.4)$$

This value is larger than the bulk lattice parameter of the STO and is close to the value of the in-plane lattice parameter derived from XRD measurement (a=3.913±0.006 Å). Similarly, also the experimentally obtained out-of-plane lattice parameter c=3.911±0.001 Å should be considered as a convolution of two contributions, one coming from slight deviation of composition and another one coming from strain induced by thermal expansion mismatch. According to the size of the in-plane lattice parameter, the out-of-plane parameter c is expected be smaller than 3.905 Å. However, the measurement showed an increase in c parameter, which can be related to the nonstoichiometry observed by several research groups.[5-7] In the RHEED pattern, taken in the [100] azimuth after subsequent continuous deposition of STO at 517°C (Fig. 4c), faint 2× reconstruction can be observed. With respect to epitaxial STO layers with the right stoichiometry, which exhibit a (1×1) surface reconstruction, these additional streaks are characteristic for Ti rich surface.[3,8,9] Resulting in the slight nonstoichiometry of STO thin films RHEED results thus correspond to the results of XRD measurements.

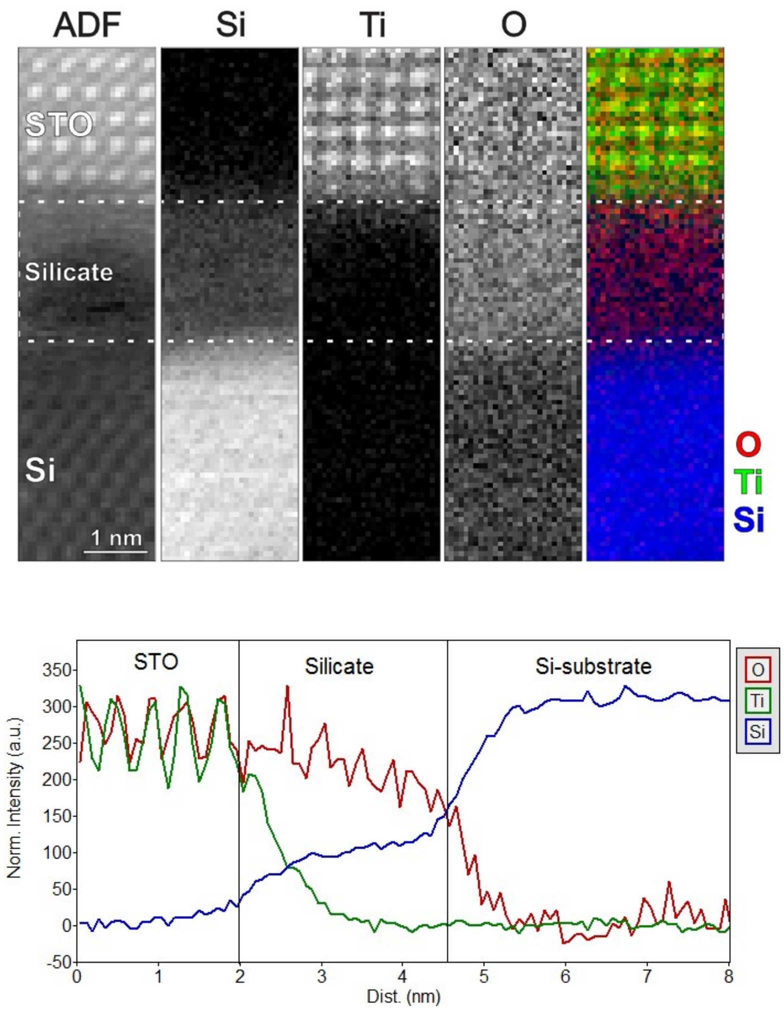

Figure S.10. TOP: Atomically resolved EELS maps of a region with high quality epitaxial STO thin film. The Si, Ti, and O elemental maps are presented in grey-scale, together with its corresponding colour map with O (red), Ti (green) and Si (blue). BOTTOM: Normalized elemental profiles, showing the presence of a silicate layer with a thickness of about 2.5nm.

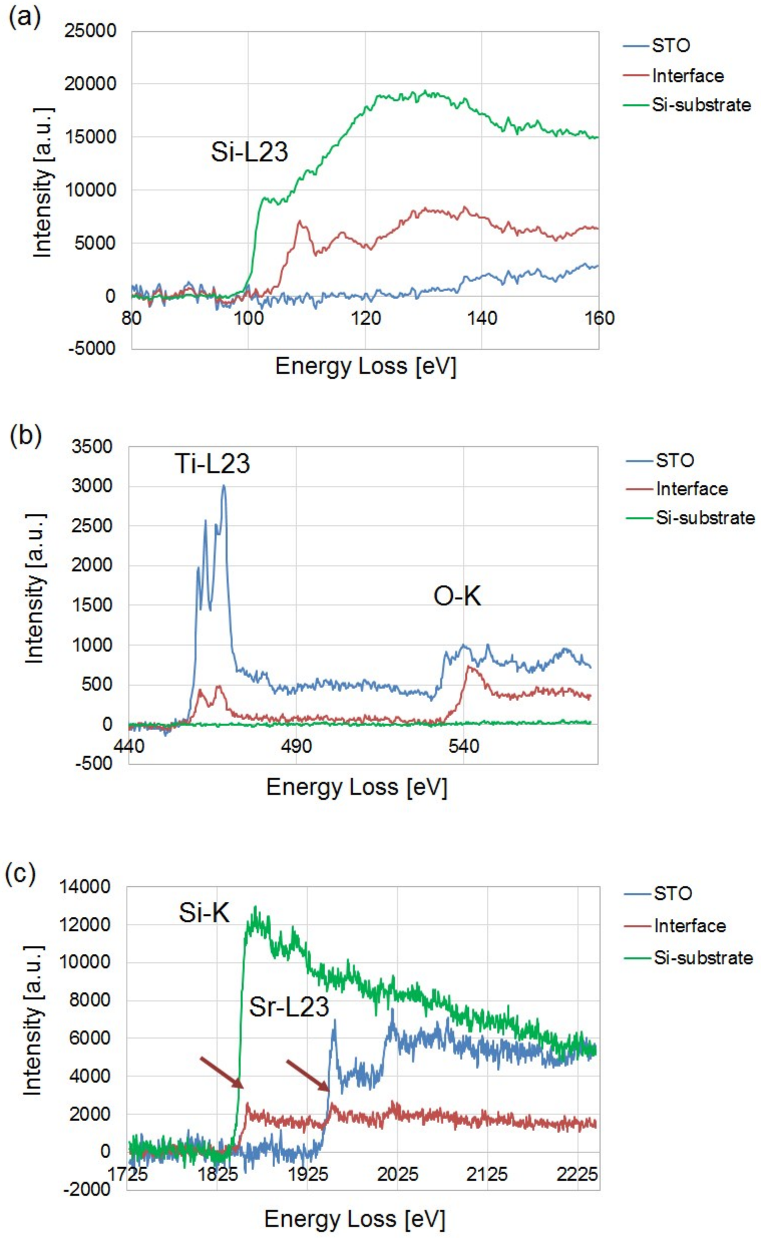

Figure S.11. ELNES of (a) Si L_{23}, (b) Ti L_{23} and O K and (c) Si K and Sr L_{23} edges. Measurements were obtained from the STO (red curve), silicate (green curve) and Si substrate (blue curve), confirming the presence of cubic perovskite structure, amorphous strontium titanium silicate phase and pure silicon, respectively. Left and right arrow in (c) points to Si and Sr at the interface, respectively.

Interface structure of epitaxial STO thin film on silicon

Results of TEM study were further compared with XRR measurement of the sample with final STO layer, which revealed some details about the STO/Si interface. In addition to equally spaced fringes indicated by arrows in Figure S.12 one very broad fringe centered at around 1.75° in omega can be observed. This additional fringe implies that there is a very thin layer present at the interface between STO and Si. The thickness of the interface layer is ~2.3 nm according to the Fourier plot, shown in the inset of Figure S.12, and thus coincides with TEM results. Our RHEED results show that 6 MLs thick amorphous STO seed layer deposited at room temperature crystallizes during the annealing at 517°C (Figure 4b). However, appearance of streaks does not exclude initial formation of an ultra-thin interface layer. We tried to confirm its presence by measuring the XPS Si 2p spectrum of the STO seed layer with thickness of only ~12 MLs (4.7 nm), in order to be able to detect the underlying Si 2p signal (Figure S.13). We found that the interface layer already forms during the crystallization steps of the STO seed layer, as shown by the broad peak centered at 2.6 eV higher binding energy compared to the elementary Si $2p_{3/2}$ peak (red curve). Such an energy difference is characteristic for silicates. There was no SiO_2 phase found in addition to silicate, as demonstrated from the comparison with XPS spectrum of Si substrate covered with native SiO_2 layer (blue curve). We attribute the formation of the interface layer to the instability of the Si/STO interface. Since the crystallization of the STO seed layer was performed in vacuum, the growth of the interface layer can occur at the expense of oxygen from the STO film.[10] However, it is expected that only a small fraction of the final silicate interface layer formed during the crystallization steps of the STO seed layer and that most of it arose during the subsequent deposition when high temperature and relatively high oxygen partial pressure were applied simultaneously.

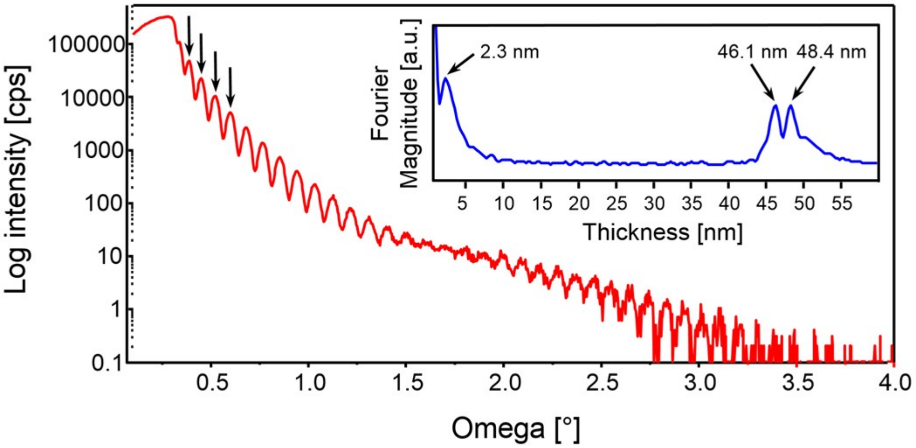

Figure S.12. XRR curve of the STO/Si sample after the final deposition with Fourier magnitude versus thickness plot in the inset.

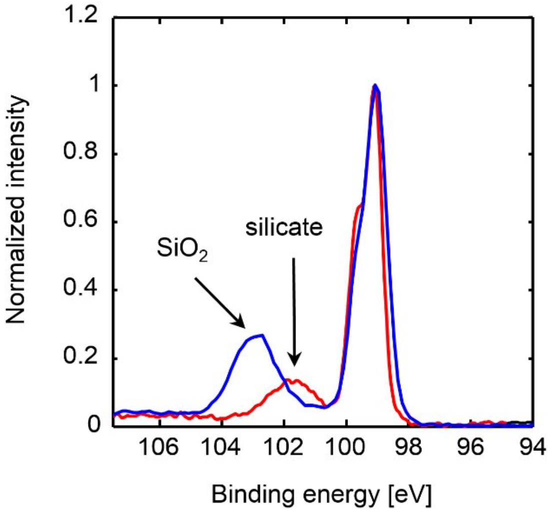

Figure S.13. XPS Si 2p spectrum measured on Si substrate covered with the native SiO_2 layer (blue curve) and on a sample containing ~4.7 nm thick STO seed layer deposited at room temperature and crystallized at 517°C (red curve).

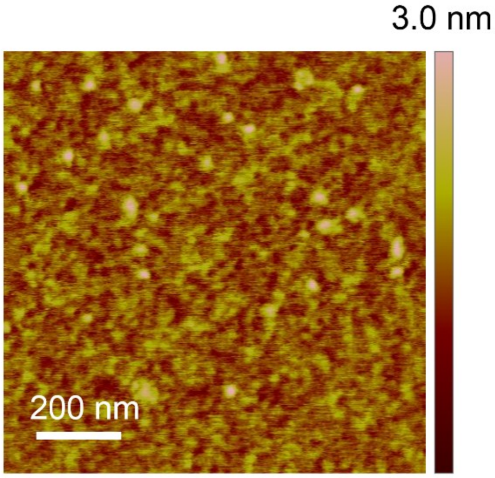

Figure S.14. AFM height image of STO/Si sample after the final deposition. The lateral scan size is 1×1 μm^2.

REFERENCES

[1] J. Heyd, G.E. Scuseria, M. Ernzerhof, Hybrid functionals based on a screened Coulomb potential J. Chem. Phys. 124 (2006) 1.

[2] J.C. Woicik, H. Li, P. Zschack, E. Karapetrova, P. Ryan, C.R. Ashman, C.S. Hellberg, Anomalous lattice expansion of coherently strained $SrTiO_3$ thin films grown on Si(001) by kinetically controlled sequential deposition, Phys. Rev. B 73 (2006) 5.

[3] M.P. Warusawithana, C. Cen, C.R. Sleasman, J.C. Woicik, Y.L. Li, L.F. Kourkoutis, J.A. Klug, H. Li, P. Ryan, L.P. Wang, M. Bedzyk, D.A. Muller, L.Q. Chen, J. Levy, D.G. Schlom, A ferroelectric oxide made directly on silicon, Science 324 (2009) 367-370.

[4] K. Munakata, A. Okazaki, Ultra-high-angle double-crystal X-ray diffractometry (U-HADOX) for determining a change in the lattice spacing: experiment, Acta Crystallogr. Sect. A 60 (2004) 33-39.

[5] D.J. Keeble, S. Wicklein, R. Dittmann, L. Ravelli, R.A. Mackie, W. Egger, Identification of A- and B-Site Cation Vacancy Defects in Perovskite Oxide Thin Films, Phys. Rev. Lett. 105 (2010) 4.

[6] S. Wicklein, A. Sambri, S. Amoruso, X. Wang, R. Bruzzese, A. Koehl, R. Dittmann, Pulsed laser ablation of complex oxides: The role of congruent ablation and preferential scattering for the film stoichiometry, Appl. Phys. Lett. 101 (2012) 5.

[7] D.J. Keeble, S. Wicklein, L. Jin, C.L. Jia, W. Egger, R. Dittmann, Nonstoichiometry accommodation in $SrTiO_3$ thin films studied by positron annihilation and electron microscopy, Phys. Rev. B 87 (2013) 11.

[8] R. Droopad, Z. Yu, H. Li, Y. Liang, C. Overgaard, A. Demkov, X. Zhang, K. Moore, K. Eisenbeiser, M. Hu, J. Curless, J. Finder, Development of integrated heterostructures on silicon by MBE, J. Cryst. Growth, 251 (2003) 638-644.

[9] Z. Yu, Y. Liang, C. Overgaard, X. Hu, J. Curless, H. Li, Y. Wei, B. Craigo, D. Jordan, R. Droopad, J. Finder, K. Eisenbeiser, D. Marshall, K. Moore, J. Kulik, P. Fejes, Advances in heteroepitaxy of oxides on silicon, Thin Solid Films, 462–463 (2004) 51-56.

[10] V. Shutthanandan, S. Thevuthasan, Y. Liang, E.M. Adams, Z. Yu, R. Droopad, Direct observation of atomic disordering at the $SrTiO_3$/Si interface due to oxygen diffusion, Appl. Phys. Lett. 80 (2002) 1803-1805.